

EFFICIENT RADIO PROPAGATION PREDICTION ALGORITHM INCLUDING ROUGH SURFACE SCATTERING WITH IMPROVED TIME COMPLEXITY

Abu S. M. Z. Kausar^{*}, Ahmed W. Reza, Kamarul A. Noordin, Mohammad J. Islam, and Harikrishnan Ramiah

Department of Electrical Engineering, Faculty of Engineering, University of Malaya, Kuala Lumpur 50603, Malaysia

Abstract—Precise modeling of radio propagation is necessary for experiencing the benefits of wireless technology for indoor environments. Among many modeling techniques, the ray tracing based prediction models become popular for indoor wireless radio propagation characterization. Though the ray tracing models are popular, their key deficiency is the slower performance. In this paper, an accelerated technique for three dimensional ray tracing using Adelson-Velski and Landis (AVL) tree data structure is introduced. Here, the AVL tree data structure is coupled with the concepts of quadrant eliminating technique (QET) and nearest neighbor finder (NNF) for optimization and fast characterization of indoor wireless communication. Surface intersection scheme (SIS) is also introduced for optimizing the ray-object intersection time. The AVL tree is used for the effective handling of the objects and environments relative information. The QET technique decreases the ray tracing time by omitting unnecessary object, while NNF decreases the ray-object intersection time by finding the nearest object in an efficient technique. For the validation of the superiority of the proposed technique, a detailed comparison is made with the existing techniques. The comparison shows that the proposed technique has 81.69% lower time consumption than the existing techniques.

Received 20 May 2013, Accepted 6 July 2013, Scheduled 15 July 2013

^{*} Corresponding author: Abu Sulaiman Mohammad Zahid Kausar (zahid04eee@hotmail.com).

1. INTRODUCTION

The advent of wireless technology and available low cost wireless transceivers has opened the door of various types of application (such as, personal communication system, wireless local area network, etc.) inside building area. For these applications, proper modeling for indoor radio propagation is essential. Although an indoor wireless communication network can be designed either by estimation through simulation or through extensive field measurements, it is preferable to use estimation through simulation. For estimation through simulation, the ray tracing based methods are very popular and widely used [1–6].

The main problem for the ray tracing based propagation prediction model is the ray-object intersection test. This test consumed the most time and resources in a ray tracing method [7]. Intersection test is performed every time after a new ray is generated and its goal is to determine whether there is a ray-object intersection or not. During intersection test, all of the objects present in the area of concern will be used to identify which one has the actual intersection. Hence, if all objects participate in this test, the ray tracing time consumed will be extremely high. To accelerate the ray tracing technique, various methods such as angular sectoring [8], KD-tree, octree, quad tree [4] and a preprocessing method are proposed [7]. However, the existing models, such as shooting and bouncing ray (SBR) [4], bi-directional path tracing (BDPT) [9], brick tracing (BT) [10], ray frustums (RF) [11], prior distance measure (PDM) [7], and space division (SD) [12] techniques require higher prediction time due to complex algorithms used. Moreover, the prediction accuracy is not so high. Some of the drawbacks of the listed techniques are: double ray counting error in SBR, incorrect result for multiple floor in BDPT, erroneous analytic reflection and transmission coefficient for corner bricks in BT, high intersection test time in BT due to considering all of the brick as a source after first Tx -brick interaction, use of high computer memory for complex environment in RF, increase of execution time due to the use of single list for storing cell id in SD, extra effort and expense for the preprocessing in PDM.

Considering all of the drawbacks of the existing technique, this paper introduced a new method based on Adelson-Velski and Landis (AVL) tree data structure, quadrant elimination technique (QET) and nearest neighbor finder (NNF). The AVL tree [13] is used for efficiently handling different information relative to the objects and scenarios. This tree has a lower data searching time, which helps to find a particular object for simulation within a shorter time and thus contributes in reduction of ray tracing time. The QET technique

helps to choose the quadrant in which the ray-object intersection will possibly occur. The objects of the chosen quadrant will only be considered for ray-object intersection test and the other three quadrants and the objects of those quadrants will be omitted. Thus, QET eliminates the unnecessary objects. The NNF technique finds the actual object, which intersects with the ray from all the object of the chosen quadrant (done by QET) and thus optimizes the ray tracing technique. This optimization uses the ‘Pythagoras Theorem’ and the newly introduced diagonal intersection point (DIP) technique for finding the actual object. Thus, it eliminates the time for the intersection test between the ray and all of the objects of the chosen quadrant. Finally, the surface intersection scheme (SIS) is used for finding the ray-object intersection point, which also optimizes the time by reducing the number of surface during intersection point calculation.

2. SCATTERING MODEL

Firstly we are going to present the model we have used for computing rough surface scattering field and then the ray tracing technique will be described with the acceleration techniques. The following model is based on the well-known Kirchhoff Approximation (KA). So the rough surface is decomposed into micro-facets, i.e., into small planes that are locally tangent to the roughness. Figure 1(a) represents an arbitrary tangent plane on a rough profile, and the notations used hereafter for the incident and the scattered fields.

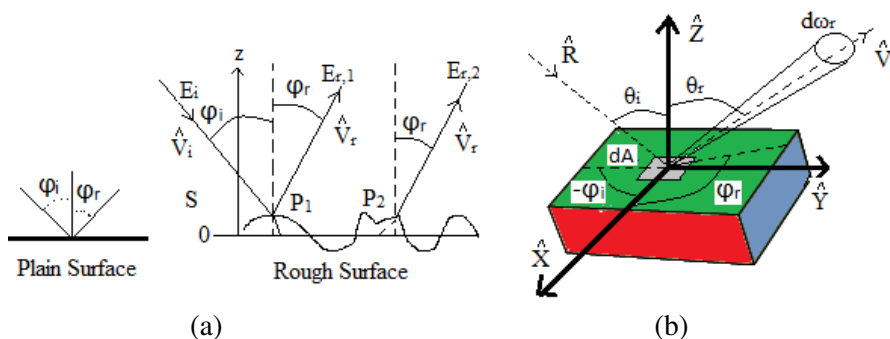


Figure 1. (a) Plain and rough surface geometry. (b) Geometry used to define surface elements.

Let us consider a rough surface geometry shown in Figure 1(a). The EM field scattered in reflection inside the surface S at the point P_1 , can be obtained by Kirchhoff-Helmholtz integral equation. From

this Kirchhoff approximation the equation can be written as [14]

$$E_{r1} = +2ik_1 \left(\bar{I} - \hat{V}_r \hat{V}_r \right) \cdot \iint dx_{P1} dy_{P1} G_1(R_{P1}, R) F_r(\gamma_{P1,x}, \gamma_{P1,y}) \times E_i(R_{P1}) \Xi_r(R_{P1}) \quad (1)$$

where, Ξ_r is the illumination function in reflection.

$$x_{P1} \in \left[\frac{-L_{Px}}{2}; \frac{+L_{Px}}{2} \right] \quad \text{and} \quad y_{P1} \in \frac{-L_{Py}}{2}; \frac{+L_{Py}}{2} \quad (2)$$

In Equation (1), the ‘Green’s function’ is used for describing the propagation of the scattered wave. Its expression is given by [14, 15]

$$G_\alpha(R, R_P) = \frac{i}{2} \int \frac{dv}{(2\pi)^2} \frac{e^{iv \cdot (r-r_P) + if(v)|z-\zeta_{Pn}|}}{f(v)} \quad (3)$$

where, $v = v_x \hat{x} + v_y \hat{y}$ and $r = x \hat{x} + y \hat{y}$ with [14]

$$f(v) = \begin{cases} \sqrt{v_\alpha^2 - \|v\|^2}; & \text{if } v_\alpha^2 \geq \|v\|^2 \\ i\sqrt{\|v\|^2 - v_\alpha^2}; & \text{if } v_\alpha^2 < \|v\|^2 \end{cases} \quad (4)$$

Now the ‘Green’s function’ can be approximated by [14]

$$G_\alpha(R, R_P) \cong \frac{\exp[i(v_\alpha R - V_s \cdot R_P)]}{4\pi R} \quad (5)$$

With $V_s = V_r$ for $\alpha = 1$.

Substituting Equation (5) to Equation (1), the ‘scattered field’ can be expressed as [14]

$$E_{r,1}^\infty = + \frac{iv_1 E_0 e^{ik_1 R}}{2\pi R} \left(\bar{I} - \hat{V}_r \hat{V}_r \right) \cdot F_r(\gamma_{P1}^0) \times \int dr_{P1} e^{i(V_i - V_r) \cdot R_{P1}} \Xi_r(R_{P1}) \quad (6)$$

where, $\int dr_{P1} \equiv \iint dx_{P1} dy_{P1}$ and $F_r(\gamma_{P1}^0)$ is given by [14], with $\gamma_{P1,x}^0$, $\gamma_{P1,y}^0$ given by

$$\gamma_{P1,x}^0 \equiv - \frac{(v_{rx} - v_{ix})}{v_{rz} - v_{iz}} \quad (7)$$

$$\gamma_{P1,y}^0 \equiv - \frac{(v_{ry} - v_{iy})}{v_{rz} - v_{iz}} \quad (8)$$

Here, the third coordinate z is used to represent the change of height of the reflected rays after reflection from a rough surface.

To define the scattering technique for our simulation environment, we have used the roughness technique proposed by ‘Oren-Nayar’ [16] which is the modification of ‘Lambertian method’ [16]. Figure 1(b) defines the parameter notations, which have been used for describing

the technique below. In Figure 1(b), θ_i marks incidence angle and φ_i marks incident azimuth angle while, θ_r denotes reflected angle and φ_r denotes reflected azimuth angle. The terminology of diffuse reflection is expressed in terms of reflected radiance L_r and incident radiance L_i . Now by considering an isotropic surface with V cavities with same facet slop θ_a and uniform distribution in orientation φ_a , the radiance can be determined as [16]

$$L_r(\theta_r, \theta_i, \varphi_r - \varphi_i; \sigma) = L_r^1(\theta_r, \theta_i, \varphi_r - \varphi_i; \sigma) + L_r^2(\theta_r, \theta_i, \varphi_r - \varphi_i; \sigma) \quad (9)$$

A modification has been done based on the term K_3 by neglecting inter-reflection. According to ‘Oren-Nayar’

$$L_r(\theta_r, \theta_i, \varphi_r - \varphi_i; \sigma) = \frac{\rho}{\pi} E_0 \cos \theta_i (A_1 + A_2 \max[0, \cos(\theta_r - \theta_i)]) \sin \alpha \tan \beta \quad (10)$$

where,

$$A_1 = 1 - 0.5 \frac{\sigma^2}{\sigma^2 + 0.33} \quad (11)$$

$$A_2 = 0.45 \frac{\sigma^2}{\sigma^2 + 0.09} \quad (12)$$

This simplified Equation (10) has advantages for using in purpose of computer simulation.

3. DETAILED RAY TRACING ALGORITHM

3.1. The Proposed QET Technique

As ray-object intersection is the most critical part in the ray tracing technique, it is necessary to find the objects which are taking part in intersection test. We have shorted the necessary objects in two different techniques. First we have used the proposed QET to find a group of objects according to the ray direction. Then the NNF will find the nearest object from that particular group of objects and that nearest object will take part in intersection test. These two acceleration techniques will reduce the intersection test time by finding the exact object. As the proposed technique is for 3D, octants have been used in the simulation tool for finding an object using the QET. The graphical representation of octants for QET is a bit complicated. So, here quadrants are used instead of octants to represent the QET. Both of the quadrants and octants are Cartesian coordinates and the basic of octants and quadrants are pretty similar [17]. The coordinate axis $x = 0$, $y = 0$ divide the plane into 4 regions called quadrants.

Similarly, the coordinate planes $x = 0$, $y = 0$ and $z = 0$ divide the space into 8 regions called octants.

In the proposed algorithm, interval between two consecutive rays shooting is one degree (1°). That means starting from zero degree it finishes at 359° . Now, first divide the surface in four quadrants (I, II, III, and IV) at the T_x position or the position of ray beginning. As we know, that the whole surface covers 360° , each of the quadrants covers 90° of the surface. That means quadrant I covers 0° to 90° , II covers 90° to 180° , III covers 180° to 270° and IV covers 270° to 360° or 0° . If the T_x position is (X, Y) then, the objects having a position $(> X, < Y)$ will be found in I, $(< X, < Y)$ in II, $(< X, > Y)$ in III and $(> X, > Y)$ in IV, where the origin of the simulation space is the top left corner. Now, based on the ray shooting angle, we can identify the quadrant in which the ray is going to travel. So, for first intersection test of that particular ray, the objects of that particular quadrant are enough to be tested. A sample environment is shown in Figure 2, which has 44 different objects, one T_x and one R_x . Suppose, a ray is shooting at an angle of 110° (which is in between 90° to 180°) from the T_x . Then it is obvious that it will travel to the quadrant II and only the objects having location $(< X, < Y)$ will be tested for intersection test. In this case, only object 26–43 will have to test for intersection test. That means 17 objects out of 44 have to test. By this way the QET eliminates objects which decrease the burden for next step.

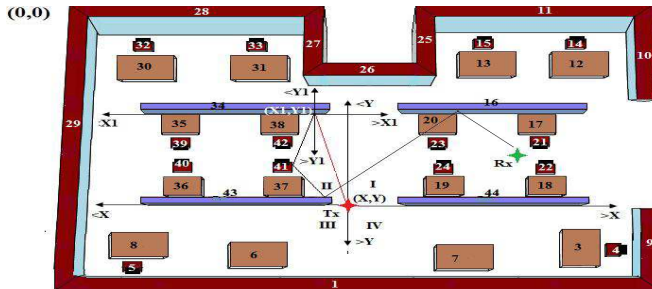


Figure 2. Sample environment showing QET and NNF.

3.2. Proposed NNF Technique

By applying the QET technique a group of possible intersecting objects can be found. Most of the objects of this group are parallel to each other. In case of this type of parallel objects, only the nearest object will take part in the intersection test. So, it will not be wise to test

all of the objects whether they are intersecting or not. It will consume time and will make the ray tracing less efficient. So, for finding this nearest object we have introduced NNF. This technique is divided into two phases. In the first phase, diagonal intersection point (DIP) (point ‘A’ in Figure 3(a)) will be calculated for each of the objects. Then, this DIP will be used to find the distance of that object from the ray source. This will be done for all of the parallel objects. After all, the decision of nearest object will be taken by comparing the distances of the parallel objects from the source ray.

The DIP is the point of intersection between two diagonal of a rectangle. Suppose, the surface containing C1, C3, C5, and C7 vertices of an object are in front of the ray source B (X2, Y2) (Figure 3(a)). Using these four vertices, two diagonals C1C7 and C3C5 can be found. The intersection point between C1C7 and C3C5 will be considered as the DIP for this object. If (x1, y1), (x3, y3), (x5, y5), and (x7, y7) are the coordinates of C1, C3, C5, and C7, respectively, then ‘the intersection point (DIP) A(X1, Y1) between two diagonals can be found as’

$$\begin{aligned}
 X1 &= \frac{\begin{vmatrix} x_1 & y_1 \\ x_7 & y_7 \end{vmatrix} \begin{vmatrix} x_1 & 1 \\ x_2 & 1 \end{vmatrix} - \begin{vmatrix} x_3 & y_3 \\ x_5 & y_5 \end{vmatrix} \begin{vmatrix} x_3 & 1 \\ x_5 & 1 \end{vmatrix}}{\begin{vmatrix} x_1 & 1 \\ x_7 & 1 \end{vmatrix} \begin{vmatrix} y_1 & 1 \\ y_7 & 1 \end{vmatrix} - \begin{vmatrix} x_3 & 1 \\ x_5 & 1 \end{vmatrix} \begin{vmatrix} y_3 & 1 \\ y_7 & 1 \end{vmatrix}} = \frac{\begin{vmatrix} x_1 & y_1 & x_1 - x_7 \\ x_7 & y_7 & x_3 - x_5 \end{vmatrix}}{\begin{vmatrix} x_1 - x_7 & y_1 - y_7 \\ x_3 - x_5 & y_3 - y_5 \end{vmatrix}}; \\
 Y1 &= \frac{\begin{vmatrix} x_1 & y_1 \\ x_7 & y_7 \end{vmatrix} \begin{vmatrix} y_1 & 1 \\ y_2 & 1 \end{vmatrix} - \begin{vmatrix} x_3 & y_3 \\ x_5 & y_5 \end{vmatrix} \begin{vmatrix} y_3 & 1 \\ y_5 & 1 \end{vmatrix}}{\begin{vmatrix} x_1 & 1 \\ x_7 & 1 \end{vmatrix} \begin{vmatrix} y_1 & 1 \\ y_7 & 1 \end{vmatrix} - \begin{vmatrix} x_3 & 1 \\ x_5 & 1 \end{vmatrix} \begin{vmatrix} y_3 & 1 \\ y_7 & 1 \end{vmatrix}} = \frac{\begin{vmatrix} x_1 & y_1 & y_1 - y_7 \\ x_7 & y_7 & y_3 - y_5 \end{vmatrix}}{\begin{vmatrix} x_1 - x_7 & y_1 - y_7 \\ x_3 - x_5 & y_3 - y_5 \end{vmatrix}}
 \end{aligned} \tag{13}$$

Now the distance between the DIP A(X1, Y1) and ray source B(X2, Y2) will be calculated by using the ‘Pythagoras Theorem’. By extending the points A and B, a right angled triangle ABC will be formed (Figure 3(a)). The coordinates of the point C will be (X1, Y2). Now, by applying the ‘Pythagoras Theorem’ in the right

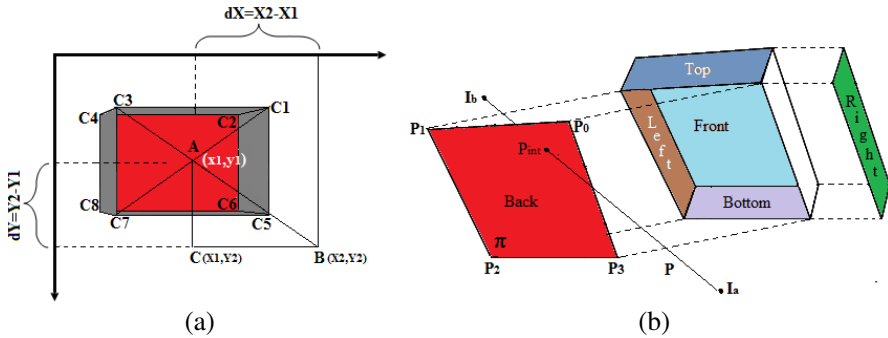


Figure 3. (a) Distance calculation between ray source and DIP. (b) Intersection point calculation between ray and a surface by using SIS.

angled triangle, we found,

$$AB^2 = AC^2 + BC^2 = (Y2 - Y1)^2 + (X2 - X1)^2 \quad (14)$$

If the distance between A and B is D , then from Equation (11), we found,

$$D = \sqrt{dX^2 + dY^2} \quad (15)$$

where, dX is the difference between the X -coordinates of A and B and dY is the difference between the Y -coordinates of A and B.

According to Figure 2, when a ray shoots in the second quadrant at an angle of 110° , the possible intersecting objects are the 28th, 31st, 33rd and 34th objects. These objects are all parallel to each other. The nearest of the four objects has to find out. For this, at first, the DIP of the objects will have to be found and it will be done by using 'Equation (13)'. Now, suppose the DIP of the 28th, 31st, 33rd, and 34th objects are A, D, E, and F, respectively. At this instant, these points will be used for calculating the distance between the objects and ray source point by using 'Equation (15)'. Suppose the distances are D_1 , D_2 , D_3 , and D_4 , respectively. Then by comparing the distances the nearest object will be chosen. In the above case, 34th object is found as the nearest object and this one will now use for an intersection test to find the intersection point.

3.3. Surface Intersection Scheme for Exact Intersection Points

After finding the nearest object, the exact ray-object intersection point is calculated by using surface intersection scheme (SIS). Based on this

intersection point the next ray shooting decision will be taken from this point. The occurrence of reflection or refraction is also dependent on this point.

Suppose, from Figure 3(b), the line of the ray P is described by two points $I_a(x_a, y_a, z_a)$, $I_b(x_b, y_b, z_b)$ and a plane π (in this case the back surface of the 34th object) is determined by 3 non co-linear points $P_0(x_1, y_1, z_1)$, $P_1(x_2, y_2, z_2)$ and $P_2(x_3, y_3, z_3)$.

Thus a general point on the line can be represented as [18]

$$L = I_a + (I_b - I_a)t; \quad t \in R \tag{16}$$

Similarly, a general point on the plane π can be found as [18]

$$P = P_0 + (P_1 - P_0)u + (P_2 - P_0)v; \quad u, v \in R \tag{17}$$

Now, the point of intersection between the line and the plane can be found by considering L equal to P . This gives the parametric equation

$$I_a + (I_b - I_a)t = P_0 + (P_1 - P_0)u + (P_2 - P_0)v \tag{18}$$

After simplification,

$$I_a - P_0 = (I_a - I_b)t + (P_1 - P_0)u + (P_2 - P_0)v \tag{19}$$

Equation (19) can be expressed in matrix form as

$$\begin{bmatrix} x_a - x_0 \\ y_a - y_0 \\ z_a - z_0 \end{bmatrix} = \begin{bmatrix} x_a - x_b & x_1 - x_0 & x_2 - x_0 \\ y_a - y_b & y_1 - y_0 & y_2 - y_0 \\ z_a - z_b & z_1 - z_0 & z_2 - z_0 \end{bmatrix} \begin{bmatrix} t \\ u \\ v \end{bmatrix} \tag{20}$$

The value of the constant t , u , and v can be found by inverting the Equation (20).

$$\begin{bmatrix} t \\ u \\ v \end{bmatrix} = \begin{bmatrix} x_a - x_b & x_1 - x_0 & x_2 - x_0 \\ y_a - y_b & y_1 - y_0 & y_2 - y_0 \\ z_a - z_b & z_1 - z_0 & z_2 - z_0 \end{bmatrix}^{-1} \begin{bmatrix} x_a - x_0 \\ y_a - y_0 \\ z_a - z_0 \end{bmatrix} \tag{21}$$

By plugging the value of t in ‘Equation (16)’ or putting the value of u and v in ‘Equation (17)’, the intersection point $P_{int}(X, Y, Z)$ can be found. Using ‘Equation (17)’, the intersection point between ray and the 34th object of Figure 2 can be calculated. Now, this intersection point will act as the source for that particular ray for finding the next ray-object intersection point. Reflection, refraction or diffraction will occur at that point according to the object property and the ray will proceed to a particular direction. Based on that direction, again QET will apply at the intersection point and next object will be found for a ray-object intersection by applying the NNF technique. This process will continue and at the end, the ray will be count either as a valid signal received by Rx or an invalid signal.

In this study, when a ray hits on any transparent object, a refracted ray will be generated. For other kind of objects, the reflected ray will be generated. The diffracted ray is generated when a ray hits on an edge of an object. In case of reflection and refraction, Snell's law [19] is used to find the direction of rays. In case of diffraction the matter is somewhat different and it is described briefly here.

Suppose that, R_i is the origin of the incident ray, P is the point of diffraction, R_d is the end point of the diffracted ray, and \vec{S} is the direction vector. So, 'the direction of the diffracted ray' can be calculated by the following equation [20]:

$$\overrightarrow{PR_i} \cdot \vec{S} = \overrightarrow{PR_d} \cdot \overrightarrow{(-S)} \quad (22)$$

Here, the direction vector \vec{S} is oriented such that $\vec{S} \times \vec{W} = \vec{N}$, where \vec{W} is a vector that lies in the plane of one of the two surfaces of the wedge and \vec{N} is the unit vector.

4. COMPLEX ANALYSIS

For M number of objects, the search operation of an AVL tree can be implemented in $O(\log_2 M)$ time.

Let, M is the number of objects, N is the number of surfaces of each 3D object, and S is the intersection testing time for the proposed method. If R numbers of intersections are required to predict each significant ray, then the total intersection testing time can be calculated by the following equation:

$$S_{\text{proposed}} = R \times N \times O(\log_2 M) \quad (23)$$

Moreover, according to QET, the proposed method can omit a significant amount of objects during each intersection test. Let, M_{QET} be the average number of omitted objects due to QET. Now, Equation (23) becomes:

$$S_{\text{proposed}} = R \times N \times O(\log_2(M - M_{\text{QET}})) \quad (24)$$

Furthermore, the NNF technique also skips objects during intersection test. Suppose, M_{NNF} be the number of objects skipped by NNF technique. Thus, 'the equation for intersection time' will be

$$S_{\text{proposed}} = R \times N \times O(\log_2(M - M_{\text{QET}} - M_{\text{NNF}})) \quad (25)$$

In addition, the SIS technique ignores 4 of the 6 surfaces from each object. That means, only 2 surfaces or 1/3 of the surfaces have to consider for intersection test, which also reduces the intersection time. Thus, Equation (25) becomes

$$S_{\text{proposed}} = R \times \frac{N}{3} \times O(\log_2(M - M_{\text{QET}} - M_{\text{NNF}})) \quad (26)$$

As, cuboids have 6 surfaces, N can be replaced by 6. In that case, Equation (26) becomes

$$S_{\text{proposed}} = 2R \times O(\log_2(M - M_{\text{QET}} - M_{\text{NNF}})) \quad (27)$$

Table 1 shows the time complexity for the proposed technique and the existing technique; from where, it is obvious that the proposed technique has a lower time complexity.

Table 1. Time complexity for finding a significant ray for different techniques.

Technique	Time Complexity
Proposed	$2R \times O(\log_2(M - M_{\text{QET}} - M_{\text{NNF}}))$
SBR	$R \times N \times O(\log_2(M - M_{\text{MT}}));$ where M_{MT} are the skipped objects due to mailbox technique
BT	$R \times N \times O(M)$
BDPT	$R \times N \times O(M)$
RF	$R \times N \times O(\log_2(M - 2^H));$ where 2^H is the order of quad tree
PDM	$R \times N \times O(M - M_{\text{PDM}} - M_{\text{BSM}});$ where M_{PDM} and M_{BSM} are the objects skipped due to prior distance measures and bounding spheres method, respectively.
SD	$R \times N \times O(M - M_{\text{SD}});$ where M_{SD} are the objects skipped by space division

5. CALCULATION OF RECEIVED POWER AND PATH LOSS

The received power at a point is calculated by using Friis transmission formula. For 3D modeling, 3D directivity data of transmitting and receiving antennas are required, which can be interpolated from measurement data along the E and H -planes [21].

When the source is smashed by the back-traced ray, ‘the received power’ can be obtained by [11]

$$P_R = |V_R|^2 / Z_0 \quad (28)$$

where,

$$V_R = \lambda \sqrt{\frac{Z_0}{4\pi} \sum G_R(\theta_R, \phi_R) \cdot \left[\frac{(h_{R,v} \hat{\theta}_R + h_{R,v} \hat{\phi}_R)}{\left[\prod A(S_{i-1}, S_i)(\bar{R}_i \text{ or } \bar{T}_i \text{ or } \bar{D}_i) e^{-jkS_i} \right]} \cdot \sqrt{\frac{\eta P_T}{4\pi}} G_T(\theta_T, \phi_T) \frac{h_{T,v} \hat{\theta}_T + h_{T,h} \hat{\phi}_T}{R} e^{-jkR} \right]} \quad (29)$$

and Z_0 is the characteristic impedance of a receiver and $G_R(\theta_R, \phi_R)$ the gain along the ray direction. Unit vectors $\hat{\theta}_R$ and $\hat{\phi}_R$ represent vectors along the elevation and azimuth directions seen from the receiving antenna coordinate, respectively. The values $h_{R,v}$ and $h_{R,h}$ represent the polarization components.

For indoor environment, the average ‘path loss’ PL (dB) for a transmitter and receiver with separation d can be represented as [22]

$$PL \text{ (dB)} = PL(d_0) + 10n \log \left(\frac{d}{d_0} \right) + \xi \quad (30)$$

where, $PL(d_0)$ is the propagation loss at the reference distance d_0 (1 m in our case), n is the propagation exponent, and ξ is a zero-mean Gaussian distributed random variable that represents the deviation from the mean value.

6. RESULTS AND DISCUSSION

With the preceding acceleration algorithms, a computer code in C# is developed to verify the efficiency. The code is implemented basically for three dimensional objects and the coordinate vectors have three components. To evaluate the performance of the proposed technique, a comparison is made with the existing methods. The comparison is made between the proposed technique and the SBR, BT, BDPT, RF, PDM and SD techniques. The drawbacks of the existing techniques have been described in Section 1. For proper comparison, five (5) different environments are chosen (one of them is shown in Figure 2). The environments are different by means of a number of objects. Some are mostly complex and some are moderate. Measurements are done in ten (10) different sampling points for each environment, by changing the Tx and Rx positions. For fair comparison, the same environments are used and all experimental settings are kept equivalent. The results obtained from 10 different sampling points of Figure 2 are represented graphically in Figure 4. Table 2 represents the overall results for all five environments. The detail of the simulation process is as follows. First, with measured antenna radiation patterns, a three dimensional radiation pattern is interpolated and stored in the memory to save the

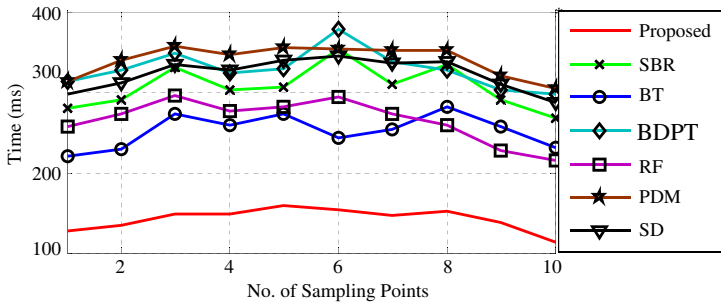


Figure 4. Comparison in terms of time.

Table 2. Combined results for all five environments.

	Time				
	1	2	3	4	5
Proposed	142	106	99	115	134
SBR	407	347	331	369	428
BT	352	304	292	316	365
RF	365	321	311	342	375
PDM	646	633	621	657	691
SD	422	376	361	398	434

calculation time. For example, bow-tie antennas of broad bandwidth at 2.4 GHz center frequency are used. The maximum gain of the antenna is 2.3 dBi. The material constants for the walls are $\epsilon_r = 9$ and $\sigma = 0 : 02$ [S/m]. The same antennas are used for the transmitter and the receiver.

According to Figure 4, the proposed algorithm shows lower time consumption for ray tracing execution. The drawbacks of the existing techniques as described before in Section 1 have been removed to decrease the time. Here, AVL tree is used for ray tracing, which decreases the time by arranging the object details in an organized approach. The QET technique also minimizes a huge amount of time by neglecting unused objects in a logical manner. The NNF and the SIS techniques reduce the ray-object intersection test time. Thus, the overall execution time becomes lower than the existing techniques. Results for all five different environments are represented in Table 2. From the results, we observe that, the proposed algorithm shows 68.35% lower time consumption than SBR algorithm, 63.38% lower than BT, 65.30% lower than RF technique, 81.69% lower than PDM method, and 70.10% lower than SD technique.

6.1. The Effect of Rough Surface Scattering and the Optimization Techniques

In this proposed technique rough surface scattering is included with ray tracing technique. Scattering factor (SF) is the key feature which has impact on scattering simulation. The reflection angle changes with respect to specular reflection due to roughness of the surface and this consequence is used in the proposed technique. Here, SF is considered as a measure of surface roughness. SF has a key impact on scattering angle. When the SF increases, the scattering angle also increases. Thus the chance of ray-object interaction increases and it increase the number of predicted rays along with the prediction time. Figure 5 shows the effect of SF on time. 3.45% increased time is needed for the increase of SF from 4 to 8 and 9.48% increased time for SF of 20. So, we can say that scattering has an effect on the time of the ray tracing technique.

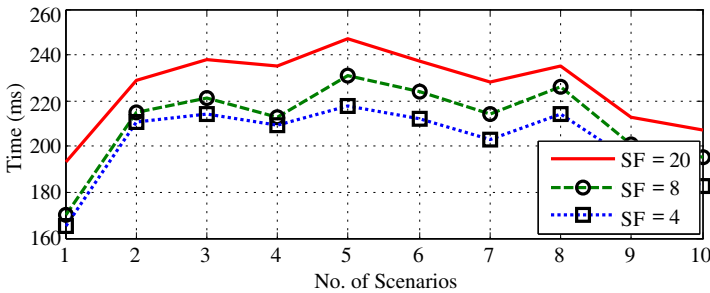


Figure 5. Change of the prediction time for different scattering factor.

Figure 6 shows the effect of scattering and the proposed optimization techniques on the ray tracing time. Here a comparative study is presented for showing the improvement of the proposed technique step by step. From Figure 6, after including the scattering in the ray tracing technique the time decreases 4.65% in average compared to without scattering (AVL) ray tracing. Furthermore, 11.68% time reduction for the inclusion of QET optimization technique and 31.55% reduction for the inclusion of both QET and NNF techniques.

Figure 6 also shows a comparison of AVL tree with Projective Scheme (PS) technique [23] and Astigmatic Beam Tracing (ABT) technique [24]. The PS technique has been used BSP tree and ABT technique has been used a beam tree. From the comparison we found that, ray tracing with AVL tree shows 20.26% less time consumption than the PS technique and 8.73% less time consumption than ABT technique. By comparing with the overall proposed technique, we

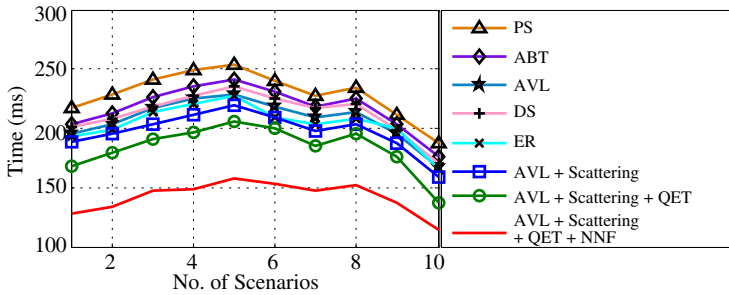


Figure 6. Effect of scattering and the proposed optimization techniques on time.

found that the proposed technique has 45.41% less time consumption than the PS and 37.53% less than ABT. Though, the ABT technique uses binary tree data structure, it stores the information about path length, curvature radius, spreading factor etc. for electromagnetic field computation [24]. So, it needs to store information for almost all of the generated rays, which results in more time consumption. On the other hand, the PS technique uses BSP tree which has a worse case time complexity of $O(n)$ for n number of nodes. With this time complexity, PS needs a higher amount of time. Furthermore, comparison with ray tracing models which have included scattering is also covers by Figure 6. Here, the proposed technique is compared with Diffuse Scattering (DS) [25] and Effective Roughness (ER) [26] models. The outcome of the comparison is that the proposed technique has 33.07% lower time requirement than DS and 30.46% lower than ER. Form the above discussion it is clear that the inclusion of AVL tree, scattering and the proposed optimization techniques are significantly reducing the ray tracing time. Although the DS and ER technique considered scattering as the proposed technique, the proposed optimization techniques make the proposed tool less time consuming.

6.2. The Influence of Tx - Rx Separation and Height

Distance between Tx and Rx and the height of Tx has a great influence on ray prediction. Here this influence has been presented graphically. Figure 7 shows the effect of Tx - Rx separation on the path loss, which is an important parameter of ray prediction technique. From the figure it is obvious that the path loss is increasing as the increasing the distance between Tx - Rx . It is also representing that, all of the considered techniques are showing a matching path loss over distance.

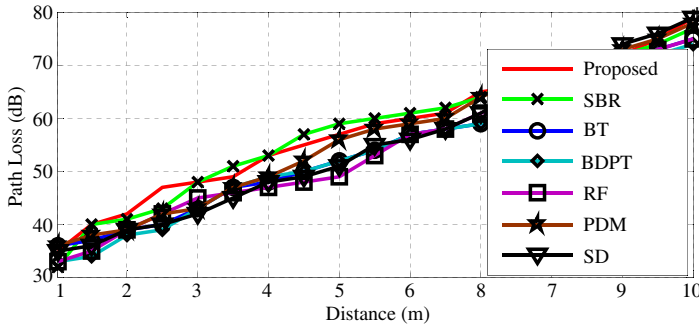


Figure 7. Distance vs path loss curve.

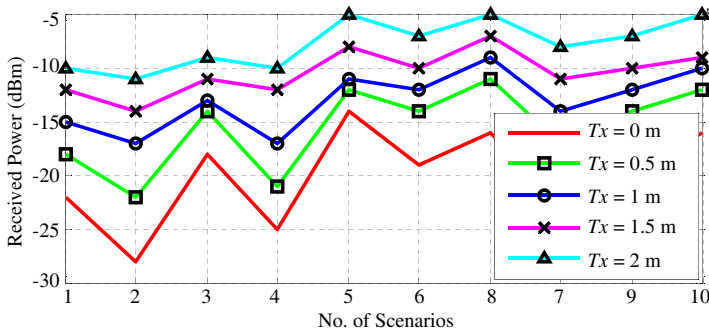


Figure 8. Change of received power with height.

This matching result verifies the proposed technique.

In Figure 8, the influence of height of the T_x is presented in terms of received power. The figure reflects that, as the T_x height is increasing, the amount of received power is also increasing. As an example, when the T_x is in ground the average received power is -20.1 dBm and it increases to -7.7 dBm for 2 m height.

7. CONCLUSION

During a ray tracing procedure, huge computation time is required for the ray-object intersection test and the data storing and retrieving procedure. In terms of overcoming these shortcomings, this study presents a new propagation prediction technique for indoor environment, where, AVL tree is used for data storing and retrieving process and QET and NNF techniques are used for accelerating the overall ray tracing process. The SIS technique used for finding the intersection point also optimizes the ray-object intersection

test. Investigations between the proposed and the existing methods demonstrated that the proposed method has lower time complexities. The results obtained reveal that the proposed technique has improved the performance in terms of lower computational time of about 81.69%. With this accomplishment, it is anticipated that the proposed propagation prediction technique has a huge potential to be used as an indoor wireless systems prediction tool.

ACKNOWLEDGMENT

This research work is supported by the University of Malaya High Impact Research (HIR) Grant (No. UM.c/625/1/HIR/MOHE/ENG/51) sponsored by the Ministry of Higher Education (MOHE), Malaysia.

REFERENCES

1. Liu, Z.-Y. and L.-X. Guo, "A quasi three-dimensional ray tracing method based on the virtual source tree in urban microcellular environments," *Progress In Electromagnetics Research*, Vol. 118, 397–414, 2011.
2. Athanasiadou, G. E., A. R. Nix, and J. P. McGeehan, "A microcellular ray-tracing propagation model and evaluation of its narrow-band and wide-band predictions," *IEEE Journal on Selected Areas in Communications*, Vol. 18, No. 3, 322–335, 2000.
3. Sarker, M. S., A. W. Reza, and K. Dimiyati, "A novel ray-tracing, technique for indoor radio signal prediction," *Journal of Electromagnetic Waves and Application*, Vol. 25, Nos. 8–9, 1179–1190, 2011.
4. Tao, Y. B., H. Lee, and H. J. Bao, "Kd-tree based fast ray tracing for RCS prediction," *Progress In Electromagnetics Research*, Vol. 81, 329–341, 2008.
5. Mphale, K. and M. Heron, "Ray tracing radio waves in wildfire environments," *Progress In Electromagnetics Research*, Vol. 67, 153–172, 2007.
6. Tayebi, A., J. Gomez, F. M. Saez de Adana, and O. Gutierrez, "The application of ray-tracing to mobile localization using the direction of arrival and received signal strength in multipath indoor environments," *Progress In Electromagnetics Research*, Vol. 91, 1–15, 2009.
7. Alvar, N. S., A. Ghorbani, and H. R. Amindavar, "A novel hybrid approach to ray tracing acceleration based on pre-processing

- & bounding volumes,” *Progress In Electromagnetics Research*, Vol. 82, 19–32, 2008.
8. Catedra, M. F., J. Perez, F. S. Adana, and O. Gutierrez, “Efficient ray-tracing techniques for three dimensional analyses of propagation in mobile communications: Application to picocell and microcell scenarios,” *IEEE Antennas and Propagation Magazine*, Vol. 40, No. 2, 15–28, 1998.
 9. Cocheril, Y. and R. Vauzelle, “A new ray-tracing based wave propagation model including rough surfaces scattering,” *Progress In Electromagnetics Research*, Vol. 75, 357–381, 2007.
 10. Thiel, M. and K. Sarabandi, “A hybrid method for indoor wave propagation modeling,” *IEEE Transactions on Antennas and Propagation*, Vol. 56, No. 8, 2703–2709, 2008.
 11. Lee, H.-S. and H. Kim, “Accelerated three dimensional ray tracing techniques using ray frustums for wireless propagation models,” *Progress In Electromagnetics Research*, Vol. 96, 21–36, 2009.
 12. Yun, Z., M. F. Iskander, and Z. Zhang, “Fast ray tracing procedure using space division with uniform rectangular grid,” *Electronics Letters*, Vol. 36, No. 10, 895–897, 2000.
 13. Larsen, K. S., “AVL trees with relaxed balance,” *Journal of Computer and System Sciences*, Vol. 63, No. 3, 508–522, 2000.
 14. Pinel, N., J. T. Johnson, and C. Bourlier, “A geometrical optics model of three dimensional scattering from a rough surface over a planar surface,” *IEEE Transactions on Antennas and Propagation*, Vol. 57, No. 2, 546–554, 2009.
 15. Chan, C. H. and Y. Shi, “Solution to electromagnetic scattering by bi-isotropic media using multilevel Green’s function interpolation method,” *Progress In Electromagnetics Research*, Vol. 97, 259–274, 2009.
 16. Oren, M. and S. Nayar, “Generalization of Lambert’s reflectance model,” *Proceedings of the 21st Annual Conference on Computer Graphics and Interactive Techniques*, ACM, 1994.
 17. Brennan, D. A., M. F. Esplen, and J. J. Gray, *Geometry*, Cambridge University Press, Cambridge, 1998.
 18. Gottwald, S., W. Gellert, M. Hellwich, H. Kustner, and H. Kastner, *VNR Concise Encyclopedia of Mathematics*, 2nd Edition, Springer, 1990.
 19. Wolf, K. B., “Geometry and dynamics in refracting systems,” *European Journal of Physics*, Vol. 16, 14–20, 1995.
 20. Tsingos, N., T. Funkhouser, A. Ngan, and I. Carlbom, “Modelling

- acoustics in virtual environments using the uniform theory of diffraction,” *Proceedings of the 28th Annual Conference on Computer Graphics and Interactive Techniques*, 545–552, 2001.
21. Gil, F., A. R. Claro, J. M. Ferreira, C. Pardelinha, and L. M. Correia, “3D interpolation method for base-station-antenna radiation patterns,” *IEEE Antennas and Propagation Magazine*, Vol. 43, No. 2, 132–137, 2001.
 22. Ahmed, B. T., J. L. M. Campos, and J. M. L. Mayordomo, “Propagation path loss and materials insertion loss in indoor environment at WiMAX band of 3.3 to 3.6 GHz,” *Wireless Personal Communications*, Vol. 66, No. 2, 251–260, 2012.
 23. Giampaolo, E. D. and F. Bardati, “A projective approach to electromagnetic propagation in complex environments,” *Progress In Electromagnetics Research B*, Vol. 13, 357–383, 2009.
 24. Giampaolo, E. D., M. Sabbadini, and F. Bardati, “Astigmatic beam tracing for GTD/UTD methods in 3-D complex environments,” *Journal of Electromagnetic Waves and Applications*, Vol. 15, No. 4, 439–460, 2001.
 25. Degli-Esposti, V., “A diffuse scattering model for urban propagation prediction,” *IEEE Transactions on Antennas and Propagation*, Vol. 49, No. 7, 1111–1113, 2001.
 26. Degli-Esposti, V., F. Fuschini, E. M. Vitucci, and G. Falciasecca, “Measurement and modelling of scattering from buildings,” *IEEE Transactions on Antennas and Propagation*, Vol. 55, No. 1, 143–153, 2007.